International Journal of Modern Physics C
Vol. 14, No. 10 (2003) 1363–1383

World Scientific
www.worldscientific.com

ON THE EVALUATION OF NOISE LEVELS FOR QUANTIZED DATA

TOMOYA SUZUKI*, TOHRU IKEGUCHI†, and MASUO SUZUKI*

*Graduate School of Science, Tokyo University of Science
1-3 Kagurazaka, Shinjuku-ku, Tokyo, 162-8601 Japan

†Graduate School of Science and Engineering, Saitama University
225 Shimo-Ohkubo, Saitama-city, 338-8570 Japan

Received 3 March 2003
Revised 8 July 2003

In recent years, quantitative methods for evaluating chaotic properties have been developed in the field of nonlinear time-series analysis. The embedding theorem, which is a mathematical background for the methods, assumes an ideal situation in which noiseless time series are observed with infinite resolution and an infinite amount of data points. However, under real situations we cannot ignore two classes of noises which are included in really observed data. The first one is observational and dynamical noises which depend on internal nonlinear systems and performance of observational instruments. The second one is quantization error included in the time series since we usually use digital computers for applying the methods. In the present paper, we derive formulae for evaluating the levels of observational and quantization noises in the case of embedding observed time series in reconstructed state spaces. By measuring a distance between noiseless and noisy attractors, we also confirm that the derived formulae are appropriate for quantifying the noise included in the reconstructed attractor.

Keywords: Quantization; observational noise; cross-point distance distribution; correlation dimension.

PACS Nos.: 05.40.Ca, 05.45.Pq, 06.20.Dk

1. Introduction

An essential goal of applying chaotic time-series analysis[1] is to understand a mathematical structure of nonlinear phenomena through an observed time series. In order to quantitatively evaluate statistical features of deterministic chaos, several indices have been proposed, for example, fractal dimensions,[2] Liapunov spectra,[3] Kolmogorov–Sinai entropies, etc.

From the viewpoint of geometric structures of dynamical systems, we can evaluate the self-similarity of attractors by estimating fractal dimensions. In particular, we can evaluate a lower bound of the degrees of freedom of the dynamical systems by estimating the fractal dimensions that evaluate geometric structures of

attractors. Thus, we can obtain the information of how many variables we need to describe the system.

From the viewpoint of dynamical structures, the orbital instability of trajectories can be studied by estimating Liapunov exponents. If the observed data are produced from a chaotic dynamical system, the maximum Liapunov exponent is at least positive. Thus, we can use Liapunov exponents to distinguish chaos from a fixed point-like, a limit cycle-like, and a torus-like behaviors. In addition, if the orbital instability of underlying dynamics of complex observed time series is strong, Liapunov exponents are large. Then, we can also use Liapunov exponents for estimating the intensity of orbital instabilities of real data.

These indices provide very important information to quantitatively understand a mathematical structure of complex phenomena. However, the following problems appear in the case of analyzing real data. First, it is unavoidable to transfer the observed analog time-series data into digital values, for example by an analog–digital converter in order to take them into digital computers,[4] that is, even if state variables are generated from a smooth dynamical system, we have to change time-series data into discrete values for numerical analyses. Second, it is often the case with real experiments that the data sets have already been polluted by a certain amount of dynamical and observational noises. As a result, the time-series data, which we can use for numerical analyses, includes these errors. The basic methods for estimating nonlinear statistics, such as fractal dimensions[2] and Liapunov spectra,[3] cannot solve essentially the problem of the existence of these noises as the embedding theorems (which give a theoretical background for applications to evaluating these statistics)[5,6] prove a sufficient condition that the transformation from the observed time series to higher dimensional state spaces is possible only under an ideal situation. Thus, in the case that the time series is corrupted by these noises, estimation accuracy becomes worse. Namely, it is very important for us to understand the levels of these noises included in the observed time-series data in advance.

As for the noise related to a dynamical system, we usually have to treat both dynamical noises (which are included in the system evolution) and observational noises (which are included in a observation process). It is also very important to evaluate levels of the dynamical noises in the case of applying chaotic time-series analysis methods. However, we do not discuss the levels of the dynamical noise in the present paper, since it is not so easy to analyze them quantitatively and to derive a formula for their levels. Thus, we treat here the dynamical noises by experimentally introducing computer simulations. It should be noted that if we use a digital computer to evolve dynamical systems, it always includes intrinsic dynamical noises since all numbers are described by integers.

In the present paper, we analytically derive the noise level by measuring normalized mean-square errors and we formulate these errors by adopting each noise level as variables in the case of one-dimensional time-series data. Second, in the case of embedding observed time-series data through the transformation by delay

coordinates, we also formulate total noise levels in reconstructing attractors. In each case, in order to estimate the plausibility of derived formulae, we measure the distance between noiseless and noisy attractors. For this purpose, we measure a cross-point distance whose concepts are introduced in Sec. 4. As a result, we confirm that these formulae offer a plausible approximation for evaluating observation and quantization noise levels.

2. The Corruption of Time-Series Data by Noise

2.1. *Dynamical systems and noisy observation*

Let us generally describe a dynamical system and an observation function by the following equations:

$$\boldsymbol{x}(t+1) = \boldsymbol{F}(\boldsymbol{x}(t)) + \boldsymbol{\phi}(t)\,, \tag{1}$$

$$\hat{\boldsymbol{z}}(t) = \boldsymbol{G}(\boldsymbol{x}(t)) + \boldsymbol{\theta}(t) = \boldsymbol{z}(t) + \boldsymbol{\theta}(t)\,, \tag{2}$$

where $\boldsymbol{F}$ is a dynamical system which is described by n-variables, $\boldsymbol{x}(t) \in \boldsymbol{M}$ is a state value in an n-dimensional manifold $\boldsymbol{M}$ at discrete time t and $\boldsymbol{\phi}$ is a dynamical noise. In the present paper, since we do not consider the existence of dynamical noises, Eq. (1) is simply replaced by $\boldsymbol{x}(t+1) = \boldsymbol{F}(\boldsymbol{x}(t))$.

Usually, we cannot observe all variables included in $\boldsymbol{M}$. Instead, we can observe an m-dimensional time series $\boldsymbol{z} \in \mathrm{R}^m$ $(m \leq n)$. The function $\boldsymbol{G}$ corresponds to an observation function: a static transformation from the state value $\boldsymbol{x}$ on $\boldsymbol{M}$ to the observed value $\boldsymbol{z}$ in R^m $(\boldsymbol{G}(\boldsymbol{x}(t)) = \boldsymbol{z}(t))$. The variable $\boldsymbol{\theta}$ in Eq. (2) is called an observational noise. Then, $\hat{\boldsymbol{z}}(t)$ is an observed state value corrupted by the observational noise.

2.2. *Observational noise*

In any observation, a certain amount of noise exists, depending on the performance of observational instruments, observational condition, skills of experimentalists, etc. For evaluating a level of the noises, it is very natural to use the following index, the signal-to-noise (S/N) ratio,[7] which is defined by

$$R[\mathrm{dB}] = 10 \log_{10} \frac{\sum_{t=1}^{N} (z(t) - \bar{z})^2}{\sum_{t=1}^{N} \eta(t)^2}\,, \tag{3}$$

where $z(t)$ is a "pure" time series generated from the dynamical system and transformed by the function G (that is, time-series data without noise), N is the length of data and $\eta(t)$ is the first observational noise, which is assumed to be Gaussian random numbers with zero mean. Then, we set various S/N ratios by changing the variance of $\eta(t)$ in Eq. (3).

2.3. *Quantization*

Next, we introduce the quantization error as a measurement noise. It is necessary to quantize the observed time-series data in order to take it into a digital computer for numerical analyses. The noise is called the quantization error. Let us describe the range F_s from the maximum value to the minimum value of the observational data, which we call Full Scale Range (FSR). To divide this range F_s is our quantization, and its minimum value L_s is called Least Significant Bit (LSB). In the case of quantization by Q[bit], L_s is given by

$$L_s = \frac{F_s}{2^Q}, \tag{4}$$

and qL_s $(q = 0, 1, \ldots, 2^Q - 1)$ are middle points in each bin of the width L_s. When the input analog amplitude is included in $[qL_s - (1/2)L_s, qL_s + (1/2)L_s)$, the output digital value becomes qL_s as shown in Fig. 1. In this quantization, the output value has the error distributed in the range $[-(1/2)L_s, +(1/2)L_s]$ to the input value. We can consider that this error follows a uniform distribution. If the input value is larger than $(2^Q - 1)L_s + (1/2)L_s$ $(= F_s - (1/2)L_s)$, we define the output digital value as $(2^Q - 1)L_s$ (thus, the quantization error in the over range becomes larger as shown in the lower plot of Fig. 1).[8]

2.4. *Normalized mean-square error*

In an ideal situation, noiseless time series is utilized for numerical analyses. In actual cases, we can only observe the time-series data corrupted by two types of noise described in the previous section.

Now, as a first measure, we use a difference between noiseless and noisy time-series data with the following normalized mean square error E. If E is larger, the accuracy of estimating nonlinear statistics gets worse:

$$E = \frac{\sqrt{(1/N)\sum_{t=1}^{N}(z(t) - \hat{z}(t))^2}}{\sqrt{(1/N)\sum_{t=1}^{N}(z(t) - \bar{z})^2}}, \tag{5}$$

where $\hat{z}(t)$ is the time-series data corrupted by the observational noise and the quantization error, and $\bar{z}$ is the mean value of $z(t)$ $(t = 1, 2, \ldots, N)$.

3. The Method for Estimating Errors in the Case of One-Dimensional Time Series Data

3.1. *Formulation of the error*

The time-series data $x(t)$ is generated from the dynamical system of Eq. (1). Then, the variable $\hat{z}(t)$ (transformed from $x(t)$ by an observation function) includes the observational noise $\eta(t)$ and includes the quantization error $\xi(t)$ by taking observed data into a digital computer. Namely, the total noise $\theta(t)$ is given by

$\theta(t) = \eta(t) + \xi(t)$. Here, we assume that the quantization level Q[bit] is known since an experimentalist can set it up freely. We also assume that F_s is known as well. In addition, we assume that the observational noise R[dB] can be estimated *a priori*, since we usually know the performance of observational instruments and experimental situations. Under the possible assumptions described above, we consider the following issue for evaluating noise levels. Let $\eta(t)$ follow a normal distribution and $\xi(t)$ follow a uniform distribution, and both have the mean value 0. Then, the time-series data which can be utilized for numerical analyses, $\hat{z}(t)$, becomes

$$\hat{z}(t) = z(t) + \eta(t) + \xi(t)\,. \tag{6}$$

By substituting Eq. (6) into Eq. (5), we obtain

$$E = \frac{\sqrt{(1/N)\sum_{t=1}^{N}(\eta(t) + \xi(t))^2}}{\sigma_z}, \tag{7}$$

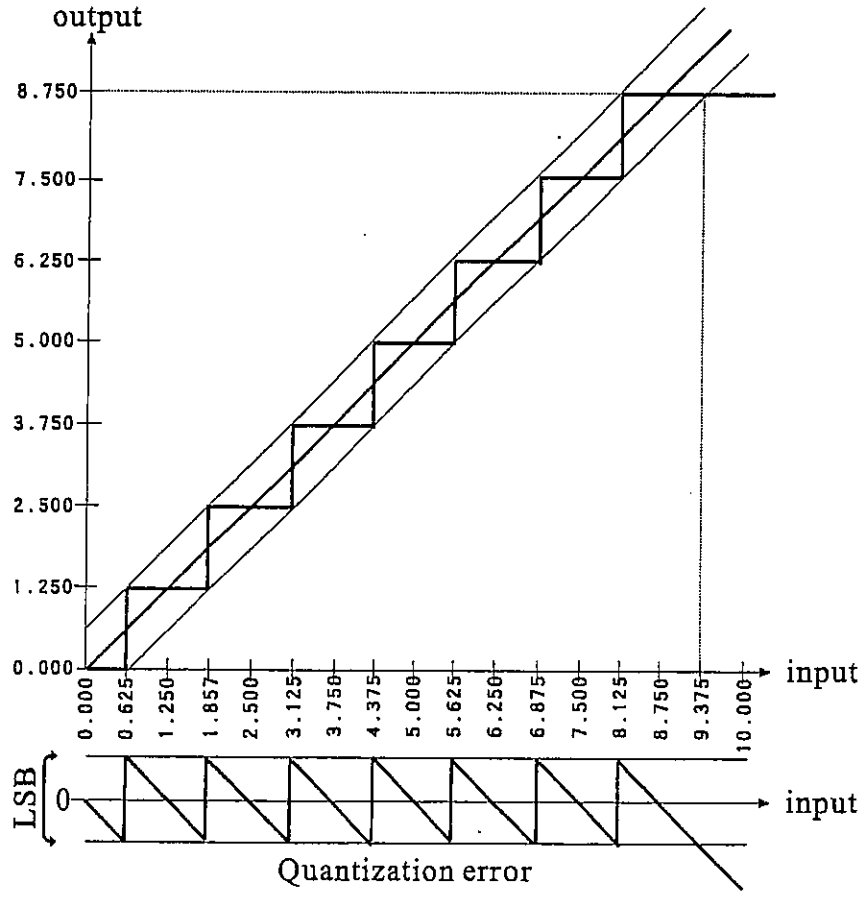

Fig. 1. The upper figure denotes the quantization characteristics of input and output data in the case of $Q = 3$[bits], $F_s = 10$ and $L_s = 1.250$. The lower figure shows the corresponding quantization errors. When the input value is larger than 9.375, the quantization output is set to 8.750.

where σ_z is the standard deviation of the time-series data $z(t)$. Without a loss of generality, Eq. (7) becomes

$$E = \frac{\sqrt{\sigma_\eta^2 + \sigma_\xi^2}}{\sigma_z}, \tag{8}$$

under the condition that $(1/N)\sum_{t=1}^{N}\eta(t)\xi(t) = 0$. Then, Eq. (3) leads us to the following results:

$$R[\mathrm{dB}] = 10\log_{10}\frac{\sigma_z^2}{\sigma_\eta^2},$$

$$\sigma_\eta^2 = \sigma_z^2 \times 10^{-R/10}.$$

Next, we calculate σ_ξ^2. Since the quantization error is considered to be uniformly distributed,

$$\sigma_\xi^2 = \frac{1}{L_s}\int_{-L_s/2}^{+L_s/2}(0-x)^2 dx = \frac{L_s^2}{12}.$$

Since $L_s = F_s/2^Q$ in Eq. (4),

$$\sigma_\xi^2 = \frac{1}{12}\left(\frac{F_s}{2^Q}\right)^2.$$

Therefore, we obtain

$$E = \sqrt{10^{-R/10} + \left(\frac{F_s}{\sqrt{12}\sigma_z 2^Q}\right)^2}, \tag{9}$$

and also we have its logarithmic representation as follows:

$$\log E = \frac{1}{2}\log\left\{10^{-R/10} + \left(\frac{F_s}{\sqrt{12}\sigma_z 2^Q}\right)^2\right\}. \tag{10}$$

However, since σ_z is an unknown quantity, it is necessary to calculate σ_z only from $\sigma_{\hat{z}}^2$, F_s, Q and R, which are assumed to be known quantities. By the additivity of variance, we have

$$\sigma_{\hat{z}}^2 = \sigma_z^2 + \sigma_\eta^2 + \sigma_\xi^2,$$

$$\sigma_z^2 = \sigma_{\hat{z}}^2 - \sigma_\eta^2 - \sigma_\xi^2 = \sigma_{\hat{z}}^2 - \sigma_z^2 \times 10^{-R/10} - \left(\frac{F_s}{\sqrt{12}\times 2^Q}\right)^2.$$

Then, we obtain the following expression:

$$\sigma_z = \sqrt{\frac{\sigma_{\hat{z}}^2 - (F_s/\sqrt{12}\times 2^Q)^2}{1+10^{-R/10}}}. \tag{11}$$

Equation (11) enables us to calculate the standard deviation of noiseless time-series data, and leads us to calculate the solution of E by substituting Eq. (11) into Eqs. (9) and (10).

3.2. *Numerical simulation*

For evaluating the above results, we perform computer simulations with the Hénon map[9]:

$$\begin{cases} x(t+1) = 1 - ax(t)^2 + y(t)\,, \\ y(t+1) = bx(t)\,. \end{cases}$$

We only use the first variable of the Hénon map $x(t)$ ($a = 1.4$ and $b = 0.3$) as an observation with the following conditions: starting from an arbitrary initial condition, we omit the first 1500 points as transients, and we use the following 2048 points for our experiments. Next, we add two types of noises to the data $x(t)$. We introduce two functions $h_R(x)$ and $h_Q(x)$ in order to describe that $x(t)$ is corrupted by $\xi(t)$ of R[dB] and by $\eta(t)$ of Q[bit]. Namely, the former adds normal random numbers as the observational noise with R[dB] to the data $x(t)$, and the latter quantizes to the data $x(t)$ by Q[bit]. Figure 2 shows the results of $\log E$ by the transformation $h_Q(h_R(x))$ with each noise. In Fig. 2, dotted lines are theoretical values calculated by Eqs. (10) and (11) and open circles are the experimental values calculated by Eq. (5) for the first variable of the Hénon map.

Next, for Eqs. (9) and (10), we consider the case of no observational noise by $R \to \infty$. Then we obtain

$$E|_{R\to\infty} = \frac{F_s}{\sqrt{12}\sigma_z 2^Q}\,, \tag{12}$$

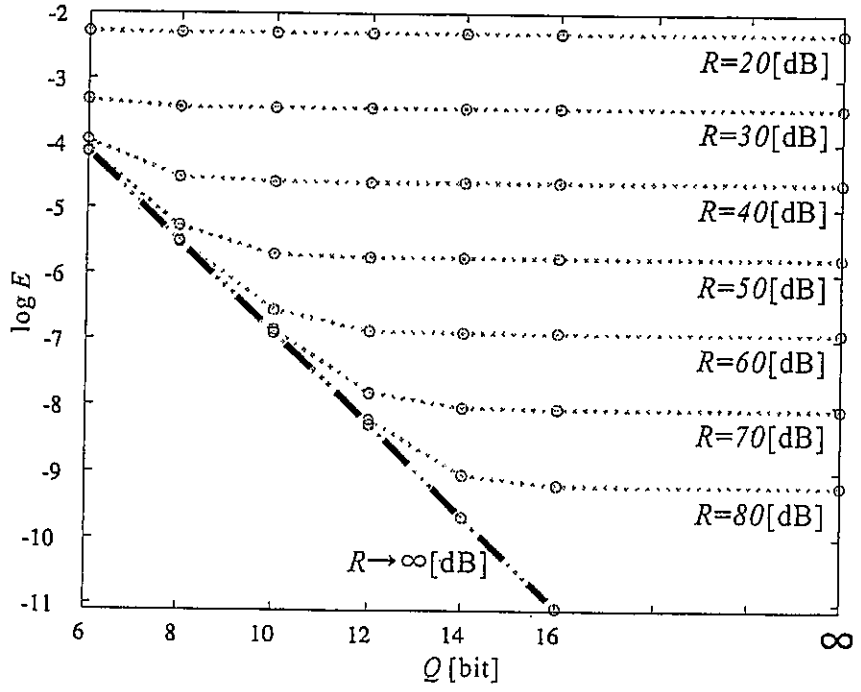

Fig. 2. Dependence of $\log E$ on Q[bit] and R[dB]. Dotted lines denote theoretical values calculated by Eqs. (10) and (11) and open circles denote experimental values estimated by Eq. (5). The first variable of the Hénon map is used for the simulation. A black dashed line denotes an asymptotic line calculated by Eq. (13).

and

$$\log(E|_{R\to\infty}) = -(\log 2)Q + \log\frac{F_s}{\sqrt{12}\sigma_z}. \tag{13}$$

Here, Eq. (13) is plotted by a dashed line in Fig. 2. On the other hand, if no quantization corresponds to $Q \to \infty$, then we have

$$E|_{Q\to\infty} = 10^{-R/20}, \tag{14}$$

and

$$\log(E|_{Q\to\infty}) = -\frac{1}{20}(\log 10)R. \tag{15}$$

Here, Eq. (15) shows the convergence of E at each observational level as shown in Fig. 2. Namely, when time-series data is corrupted by the observational noise, we cannot obtain time-series data with higher quality than that of a saturated value $\log E|_{Q\to\infty}$ shown by Eq. (15). The difference from convergence values can be calculated by subtracting Eq. (15) from Eq. (10),

$$\begin{aligned}\log E - \log(E|_{Q\to\infty}) &= \frac{1}{2}\log\left\{10^{-R/10} + \left(\frac{F_s}{\sqrt{12}\sigma_z 2^Q}\right)^2\right\} + \frac{1}{20}(\log 10)R \\ &= \frac{1}{2}\log\left\{1 + \left(\frac{F_s}{\sqrt{12}\sigma_z}\right)^2 \frac{10^{R/10}}{4^Q}\right\}.\end{aligned} \tag{16}$$

From Eq. (16) and Fig. 2, we find that the difference from the convergence value decreases exponentially as Q increases under the situation that R are constant. Namely, even if we expend numerical cost to increase the quantization level, we cannot sufficiently reduce the quantization error.

Generally, in quantization, since we perform 2^Q-times calculations per a datum, we define a numerical cost C as

$$C = N \times s \times 2^Q, \tag{17}$$

where N is a data length and s is computation speed which depends on an analog-to-digital converter. When we increase the quantization level, the improvement of $\log E$ against the growth of the numerical cost is evaluated by

$$-\frac{d\log E/dQ}{dC/dQ} = \frac{(F_s/\sqrt{12}\sigma_z)^2 \times 10^{R/10}/N \times s}{8^Q + (F_s/\sqrt{12}\sigma_z)^2 \times 10^{R/10} \times 2^Q}.$$

Since it is a decreasing function, increasing the quantization level leads to reduction of cost performance. Though the best cost performance is given by setting $Q = 0$, its data accuracy becomes worst. Namely, it is not an optimization problem for obtaining an optimum quantization level, but it becomes a trade-off between the data accuracy and the cost performance. From this point, Eq. (16) gives us valuable information on how much the normalized mean-square error can be reduced, depending on the situation.

4. Estimating Errors in the Case of Reconstructing Attractors in A Higher-Dimensional State Space

In the previous section, we estimate an error between noiseless and noisy single time series. In this section, we estimate an error between noiseless and noisy attractors in a higher-dimensional state space. In order to estimate this error, we consider "difference" between a noiseless attractor and a noisy attractor. Since it is natural to consider that the "difference" is a distance between two attractors in the state space, we should evaluate the distance under some metric with compact support between two attractors. For evaluation between two or more sets, there are Hausdorff measure, Kolmogorov measure, and so on. Although these measures are mathematically rigorous, it is convenient for us to introduce a different method based on inter-point distances[10] and cross-point distance[11,12] of points on the attractors, which would be easier for numerical calculation. We use these indices as a new distance in order to evaluate the difference between noiseless and noisy attractors in the reconstructed state space.

4.1. *Inter-point and cross-point distances*

First, we reconstruct time-series data in an m-dimensional reconstructed state space,[5] and calculate the inter-point distances on the attractor $\boldsymbol{v}(t) = \{v(t), v(t+1), \ldots, v(t+m-1)\}$ by

$$d_{kl} = |\boldsymbol{v}(k) - \boldsymbol{v}(l)| \quad (k \neq l)\,. \tag{18}$$

We introduce the condition $k \neq l$ to omit the case that $d_{kl} = 0$ since this case does not reflect the geometric feature of the attractor. Then, we calculate its frequency distribution. Here, the ith bin is defined by $B_i = [r_{i+1}, r_i)$, $i > 0$, $r_i = \lambda^i r_0$, $\lambda < 1$, and r_0 (> 0) is the cutoff value and the number of points included in B_i is denoted by b_i.[13]

Next, we can observe visually the difference between two attractors embedded in the same state space. Let us describe the first attractor $\boldsymbol{v}(t) = \{v(t), v(t+1), \ldots, v(t+m-1)\}$, and the second attractor $\boldsymbol{w}(t) = \{w(t), w(t+1), \ldots, w(t+m-1)\}$. Then, to calculate the difference between two attractors, we modify Eq. (18) as follows[11,12]:

$$d'_{kl} = |\boldsymbol{v}(k) - \boldsymbol{w}(l)| \quad (k \neq l)\,, \tag{19}$$

which we call a cross-point distance. In this case, d'_{kl} is normalized by $\max_{k,l}\{d'_{kl}\}$. Then, we calculate its frequency distribution as well as that of d_{kl}. If two attractors are the same $(\{\boldsymbol{v}\} = \{\boldsymbol{w}\})$, the distribution of the cross-point distances between two attractors d'_{kl} is equivalent to that of d_{kl}, the distribution of the inter-point distances from a single attractor. Therefore, by calculating distributions of d'_{kl} and d_{kl} and comparing these two distributions, it is possible to estimate the difference between two attractors.[11,12] For fair comparison, we impose the condition $k \neq l$ in order to normalize d_{kl} and d'_{kl}. Then, we apply the above strategy to the evaluation

of the observational noises and quantization errors in this case. Namely, we consider the first attractor $\{v\}$ as a noiseless attractor, and the second attractor $\{w\}$ as noisy attractors.

4.2. *Numerical experiments*

For numerical experiments, we introduce several examples. The first one is the Hénon map as already introduced in Sec. 3.2. The second example is the Ikeda map[14] described by:

$$\begin{cases} x(t+1) = q + b(x(t)\cos(\phi(t)) - y(t)\sin(\phi(t))), \\ y(t+1) = b(x(t)\sin(\phi(t)) + y(t)\cos(\phi(t))), \end{cases}$$

where $\phi(t) = \kappa - \alpha/(1 + x^2(t) + y^2(t))$, $q = 1$, $b = 0.9$, $\kappa = 0.4$ and $\alpha = 6.0$.

The third one is the Lorenz equations[15]:

$$\begin{cases} \dfrac{dx}{dt} = -\sigma x + \sigma y, \\ \dfrac{dy}{dt} = -xz + \gamma x - y, \\ \dfrac{dz}{dt} = xy - bz, \end{cases}$$

where $\sigma = 10$, $b = 8/3$ and $\gamma = 28$.

Finally, we use the Rössler equations[16]:

$$\begin{cases} \dfrac{dx}{dt} = -y - z, \\ \dfrac{dy}{dt} = -x + ay, \\ \dfrac{dz}{dt} = b + z(x - c), \end{cases}$$

where $a = 0.36$, $b = 0.4$ and $c = 4.5$.

We only use the first variable of each dynamical system as an observation with the following conditions: starting from an arbitrary initial condition, we omit the first 1500 points as transients, and we use the following 2048 points for our experiments. For evaluating noise level, the attractor reconstructed in an m-dimensional state space by the first variable of the above dynamical systems is considered as $\{v\}$. Then, the corrupted attractor becomes $\{w\} = h_Q(h_R(\{v\}))$. Figure 3 shows examples of $\{w\}$ ($m = 2$) of the Hénon map, with the observational noise by $R = 30$[dB] and the quantization error by $Q = 6$[bits].

Next, we calculate frequency distributions of d'_{kl}. When $\{v\}$ is equivalent to $\{w\}$ (for $R \to \infty$ and $Q \to \infty$), the frequency distributions become the same as the frequency distributions of the inter-point distance d_{kl}. They are shown in solid lines in Figs. 4–7.

In Figs. 4–7, we can confirm that the frequency distributions have different slopes and/or exhibit fluctuation from a certain scale caused by the influence of two types

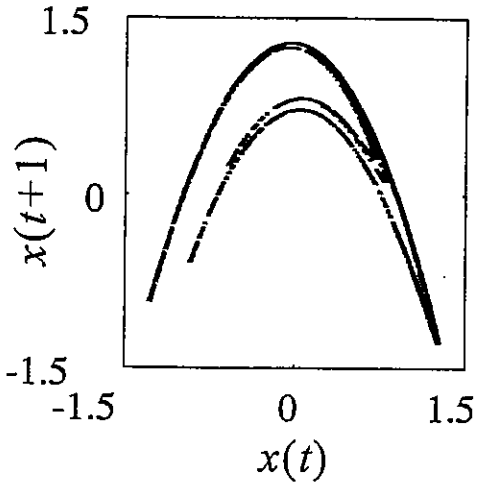

(a) $R \to \infty$[dB] and $Q \to \infty$[bits] (noiseless).

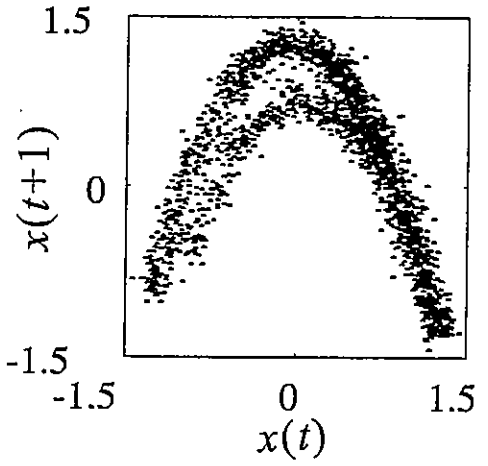

(b) $R = 30$[dB] and $Q \to \infty$[bits].

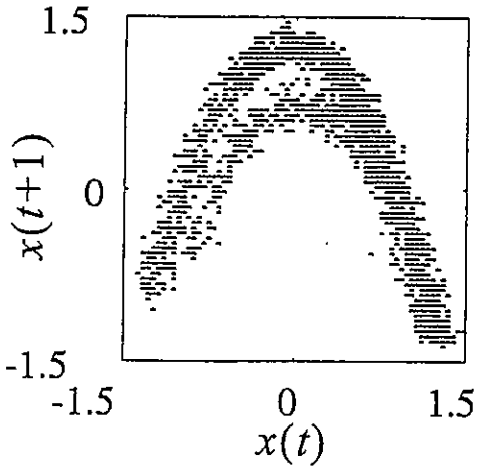

(c) $R = 30$[dB] and $Q = 6$[bits].

Fig. 3. The first variable $x(t)$ of the Hénon map is artificially corrupted by the noise levels R[dB] and the quantization levels Q[bit], and it is transformed to the two-dimensional state space $(x(t), x(t+1))$.

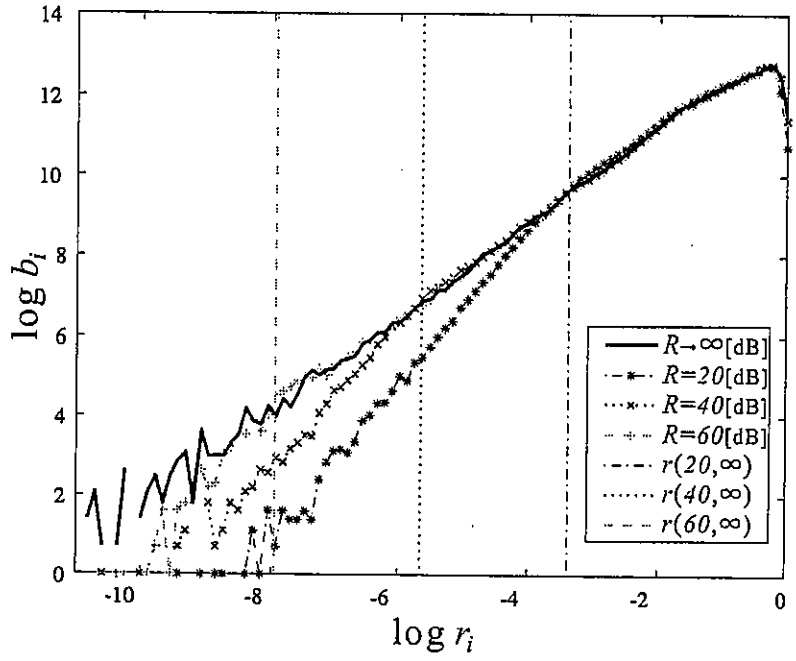

(a) $Q \to \infty$[bits].

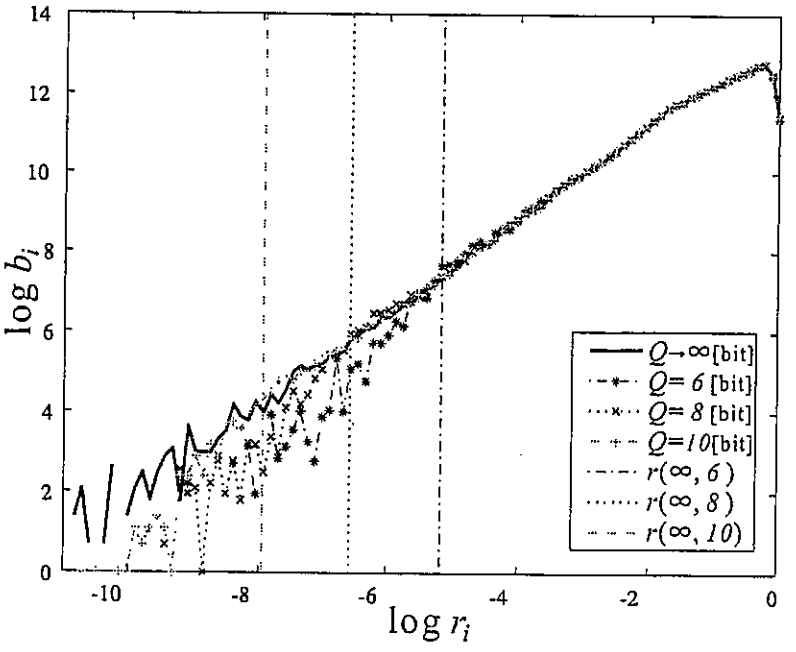

(b) $R \to \infty$[dB].

Fig. 4. In the case of the Hénon map, the frequency distributions of inter-point and cross-point distances, with $\{v\}$ and $\{w\}$ $(= h_Q(h_R(\{v\})))$, in the same state space $(m = 2)$. Solid lines correspond to the frequency distribution of the inter-point distance of $\{v\}$ (in this case $\{w\} = \{v\}$). By comparing solid lines with other frequency distributions (dashed-dotted lines, dotted lines and dashed lines), it is possible to see visually the difference between $\{v\}$ and $\{w\}$. In each figure, $r(R, Q)$'s of Eq. (21) are also plotted, which give us the information on derived critical scales, where each structure of attractors begins to be destroyed by noise of R[dB] and Q[bit]. We find that these $r(R, Q)$'s show proper values.

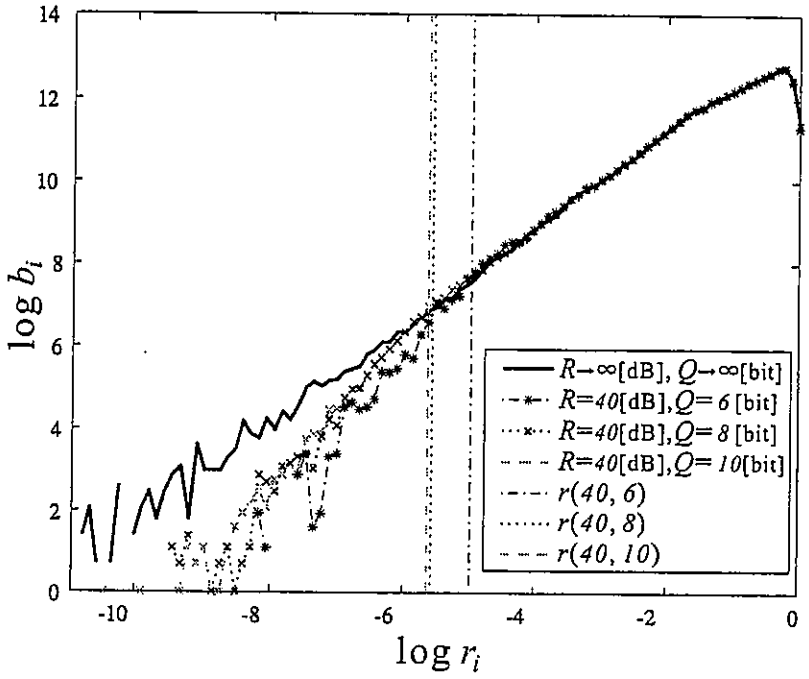

(c) Results obtained by changing R[dB] and Q[bits] simultaneously.

Fig. 4 (*Continued*).

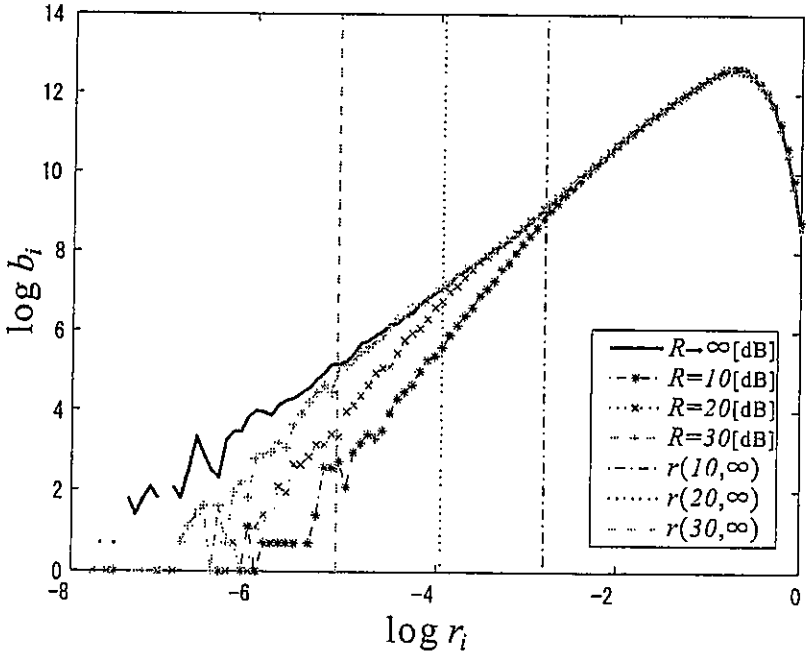

(a) $Q \to \infty$[bits].

Fig. 5. The same as Fig. 4, but for the Ikeda map ($m = 3$).

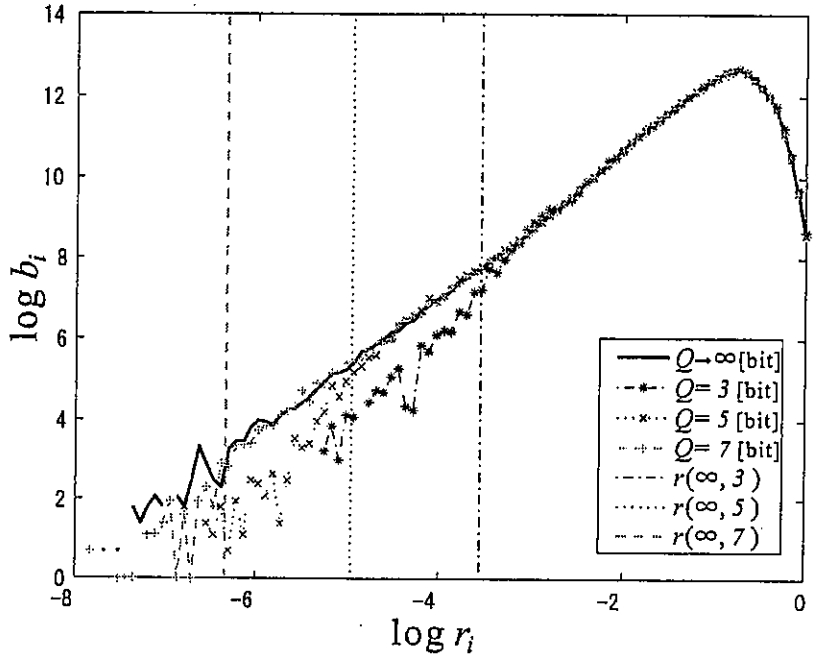

(b) $R \to \infty$[dB].

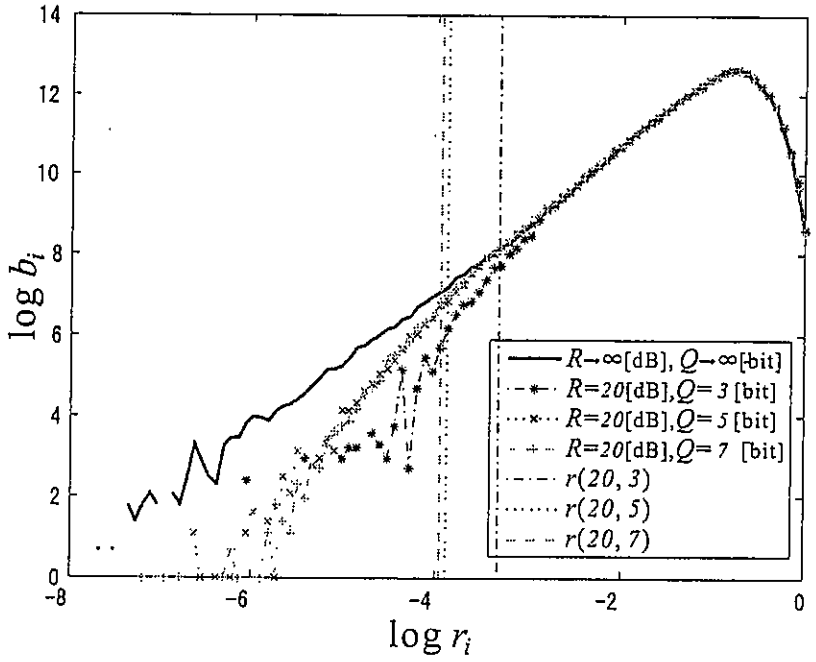

(c) Results obtained by changing R[dB] and Q[bits] simultaneously.

Fig. 5 (*Continued*).

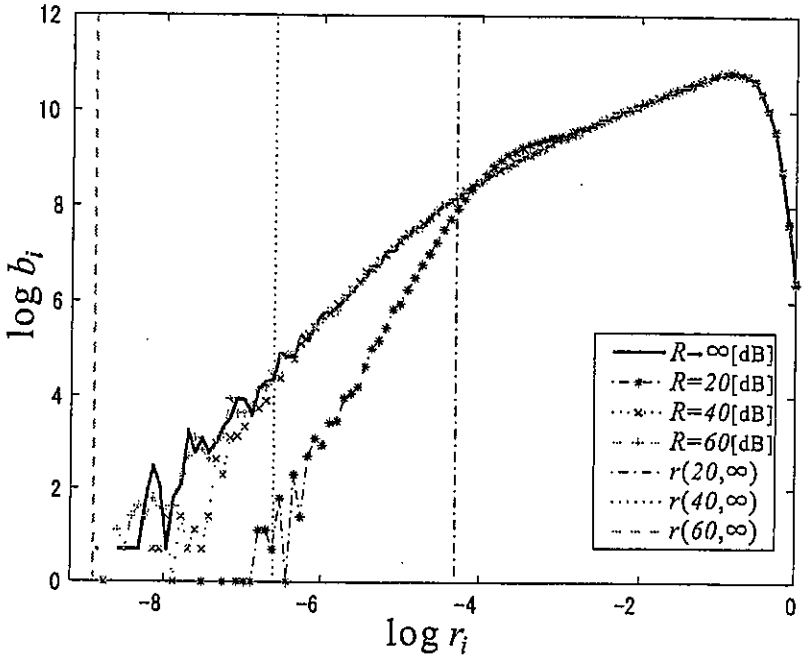

(a) $Q \to \infty$[bits].

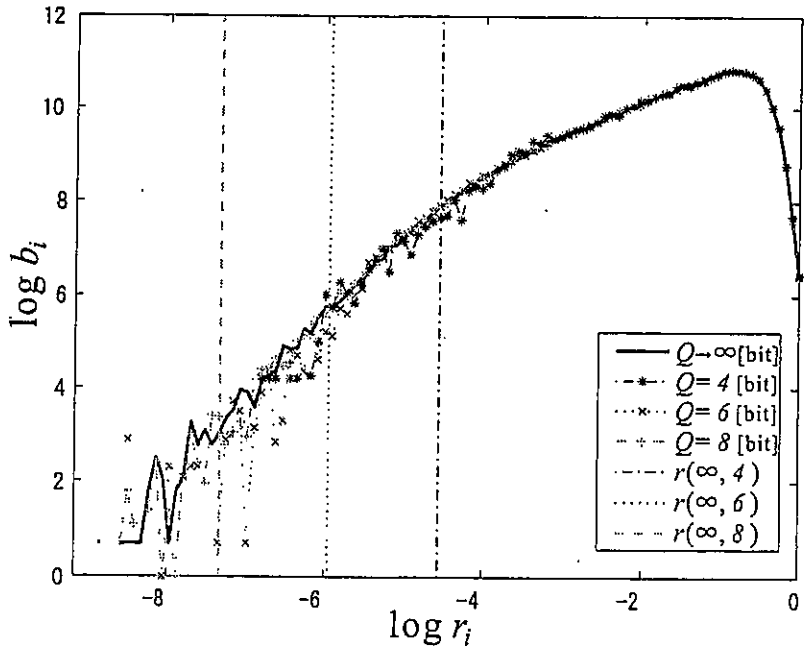

(b) $R \to \infty$[dB].

Fig. 6. The same as Fig. 4, but for the Lorenz equations ($m = 3$). In (a), since $r(60, \infty)$ is smaller than the minimum range of frequency distribution, its distribution is not disturbed by observational noise in the scales.

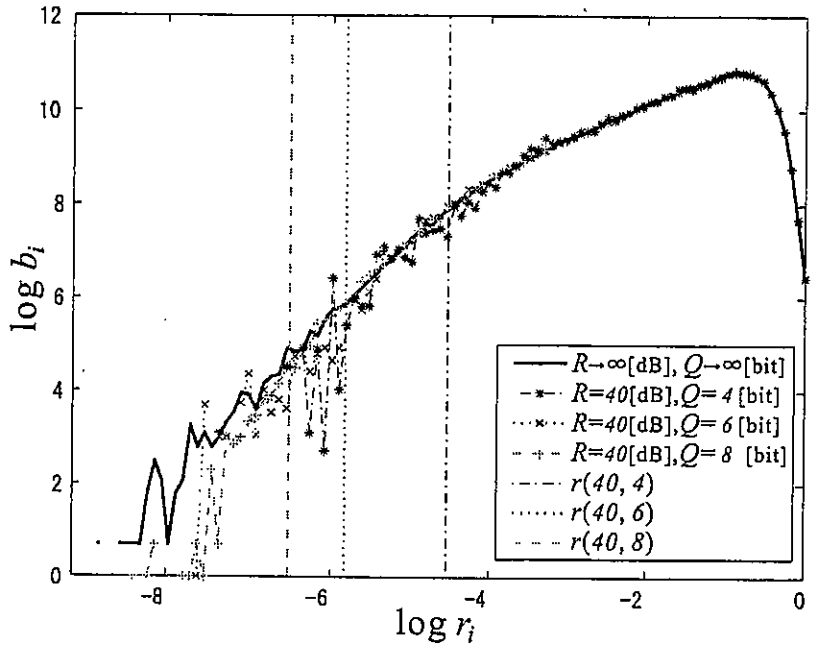

(c) Results obtained by changing R[dB] and Q[bits] simultaneously.

Fig. 6 (*Continued*).

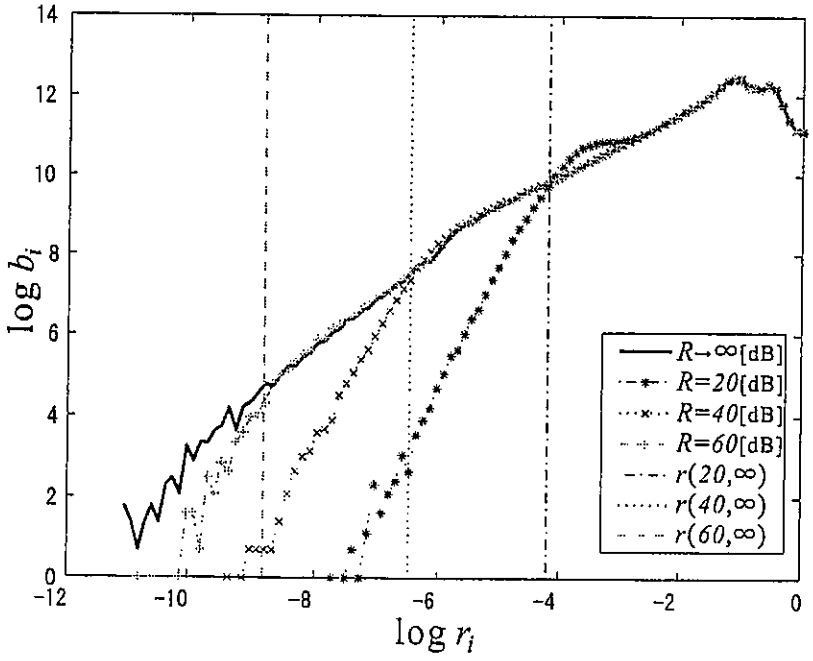

(a) $Q \to \infty$[bits].

Fig. 7. The same as Fig. 4, but for the Rössler equations ($m = 3$).

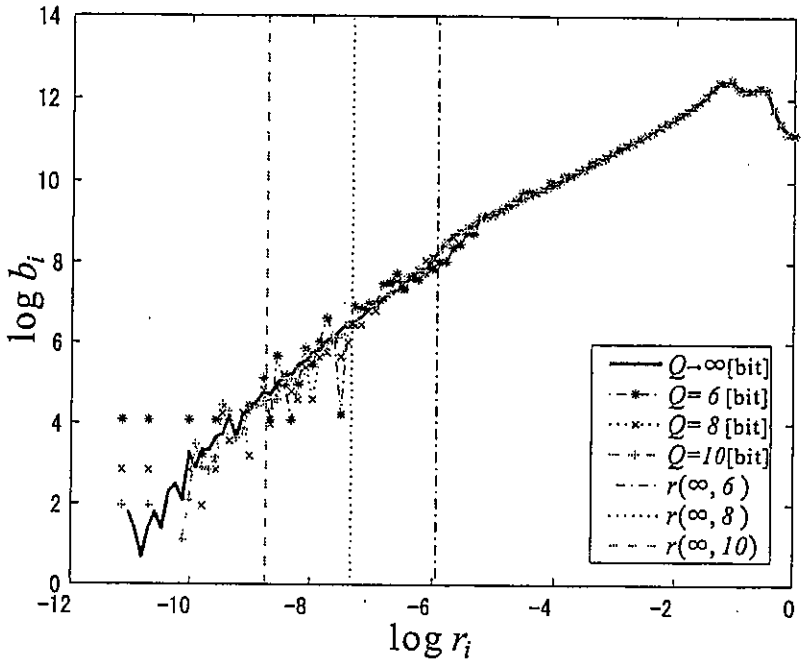

(b) $R \to \infty$[dB].

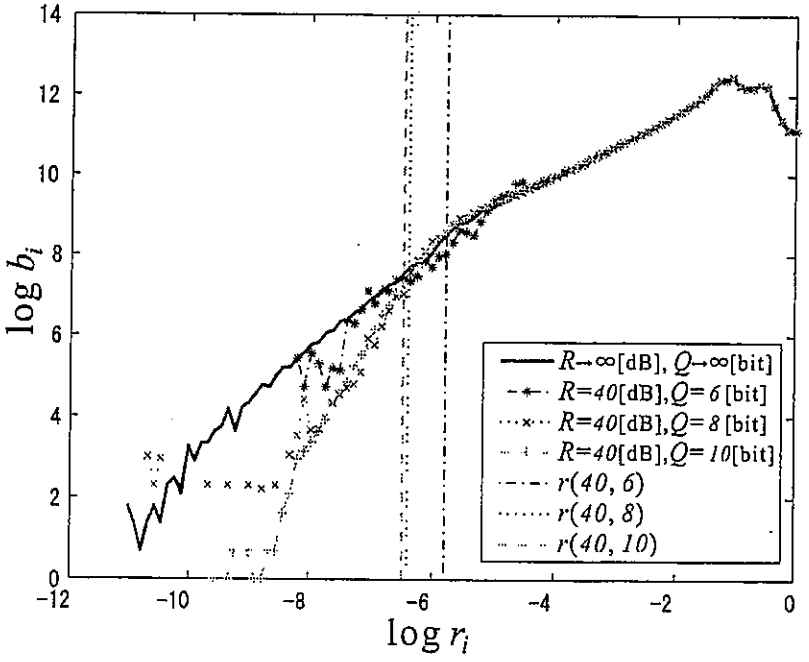

(c) Results obtained by changing R[dB] and Q[bits] simultaneously.

Fig. 7 (*Continued*).

of noise. In small scale regions, the frequency distribution is easily influenced by noise, which is similar to the case that the time series is perturbed by an additive-random noise.[17] This tendency is clearly shown by the fact that the cross-point distances are disturbed by noise.

In Figs. 4(a)–7(a), the dimension of observational noise takes a value almost m, since the transformation of Gaussian noises in a delay coordinate fills in the m-dimensional state space. Then, in the scale of strong influence of noise, the slope of a frequency distribution of the cross-point distances converges to m, since original structures of attractors are destroyed. Moreover, the inter-point distance of destroyed structures becomes large by noise and goes out in this scale.

In Figs. 4(b)–7(b), the frequency distributions are blurred by quantization noise from this scale although these tendencies are not clearer than the above cases of observational noises. In particular, the types of fluctuated distributions are different between the cases of difference equations (Figs. 4 and 5) and differential equations (Figs. 6 and 7). Though, in the former case, their frequency distributions are bended, in the latter case, their frequency distributions are disturbed. Even if we change embedding dimension, these tendencies are the same.

Figures 4(c)–7(c) correspond to real situation in which we record the observational time series by setting a quantization level. We can confirm that increasing quantization levels leads to the convergence of the frequency distributions disturbed by two types of noise (Figs. 4(c)–7(c)) to those of only observational noises (Figs. 4(a)–7(a)).

From the above simulations, we can find that there exists a critical scale, at which the structure of attractors is destroyed by the noise levels R and Q. This scale give us important information to quantify the degree of these noise. We will formulate this critical scale in the following section.

4.3. *Evaluating the critical scale*

First, we remember that the total noise in one-dimensional time series data is $\theta(t) = \eta(t) + \xi(t)$. We can also denote the noise as $\theta_i(t)$, which affects a single component on the m-dimensional reconstructed attractor $\boldsymbol{w}(t)$:

$$\theta_i(t) = \eta_i(t) + \xi_i(t)\,,$$

where $i = 1, 2, \ldots, m$, $\theta_i(t) = \theta(t + (i-1)\tau)$ and τ is a time delay. Then, we denote the global-total noise $\Theta(t)$, which is included in a global attractor $\boldsymbol{w}(t)$ and affects a cross-point distance (Eq. (19)), as

$$\Theta(t) = \pm\sqrt{\sum_{i=1}^{m}\theta_i^2(t)}\,.$$

Here, since $(1/N)\sum_{t=1}^{N}\Theta(t)=0$, the variance σ_Θ^2 is given by

$$\sigma_\Theta^2=\frac{1}{N}\sum_{t=1}^{N}\Theta^2(t)=\frac{1}{N}\sum_{t=1}^{N}\sum_{i=1}^{m}\theta_i^2(t)=\sum_{i=1}^{m}\sigma_{\theta_i}^2=m\times\sigma_\theta^2\,.$$

Moreover, since $\sigma_\theta^2=\sigma_\eta^2+\sigma_\xi^2$, the standard deviation σ_Θ is given by

$$\sigma_\Theta=\sqrt{m}\times\sqrt{\sigma_\eta^2+\sigma_\xi^2}\,. \tag{20}$$

By Eq. (8),

$$\sigma_\Theta=\sqrt{m}\times\sigma_z E\,.$$

Dividing σ_Θ by the maximum of cross-point distances, $\max_{k,l}\{d'_{kl}\}$, in a log scale, we approximate the critical scale as follow. Let us denote the approximated critical scale as $r(R,Q)$ (since it depends on both of noise levels R and Q). Therefore, we define

$$r(R,Q)=\log\frac{\sigma_\Theta}{\max_{k,l}\{d'_{kl}\}}=\log E+\log\frac{\sqrt{m}\sigma_z}{\max_{k,l}\{d'_{kl}\}}\,. \tag{21}$$

From Eq. (21), we find that $r(R,Q)$ in an m-dimensional state space has a linear relation to $\log E$ in the one-dimensional case. The calculated $r(R,Q)$'s are shown in Figs. 4–7 by vertical lines. In each figure, we confirm that a turning edge at each frequency distribution can be approximated by the derived critical scale $r(R,Q)$.

Furthermore, by Eq. (13), the asymptotic state of $r(R,Q)$ in the case of $R\to\infty$ is derived as follows:

$$\begin{aligned}r(\infty,Q)&=\log(E|_{R\to\infty})+\log\frac{\sqrt{m}\sigma_z}{\max_{k,l}\{d'_{kl}\}}\\&=-(\log 2)Q+\log\frac{F_s}{\sqrt{12}\sigma_z}+\log\frac{\sqrt{m}\sigma_z}{\max_{k,l}\{d'_{kl}\}}\\&=-(\log 2)Q+\log\frac{F_s}{\max_{k,l}\{d'_{kl}\}}\sqrt{\frac{m}{12}}\,.\end{aligned} \tag{22}$$

Then, by Eq. (15), the convergence value of $r(R,Q)$ in the case of $Q\to\infty$ is

$$\begin{aligned}r(R,\infty)&=\log(E|_{Q\to\infty})+\log\frac{\sqrt{m}\sigma_z}{\max_{k,l}\{d'_{kl}\}}\\&=-\frac{1}{20}(\log 10)R+\log\frac{\sqrt{m}\sigma_z}{\max_{k,l}\{d'_{kl}\}}\,.\end{aligned} \tag{23}$$

The difference of $r(R,Q)$ from the convergence value is given by

$$\begin{aligned}r(R,Q)-r(R,\infty)&=\log E+\frac{1}{20}(\log 10)R\\&=\frac{1}{2}\log\left\{1+\left(\frac{F_s}{\sqrt{12}\sigma_z}\right)^2\frac{10^{R/10}}{4^Q}\right\}\,,\end{aligned} \tag{24}$$

which becomes the same as Eq. (16). By Eqs. (24) and (17), it is possible to set up the quantization level Q from the viewpoint of considering numerical costs for quantization and estimating error on a multi-dimensional attractor.

Finally, it is valuable to comment on the multi-dimensional case. Namely, it is easy to extend the above formulae in the case of multivariables of time-series data embedded in a reconstructed state space,[5] if we consider σ_Θ^2 as the sum of each variance of total noise included in each variable in Eq. (20).

5. Conclusions

In the present paper, we have formulated the influence of noise in the following cases: one-dimensional time series and a reconstructed attractor from the one-dimensional time series in multi-dimensional state space. In each case, we have shown the plausibility of these formulae by comparing each experimental result with our theoretical one. Then, we have found that increasing quantization level does not always lead efficiently to the reduction of total errors. We have also shown that the influence of the noise in the case of reconstructed attractors in a multi-dimensional state space has a linear relation to the case of one-dimensional time-series data. These results are expected to be good guidelines to set up appropriate quantization levels with considering numerical costs for nonlinear, possibly chaotic time-series analysis.

Acknowledgments

The authors would like to thank Y. Horio, M. Adachi, and K. Jinno for their valuable comments and discussions. The research of TI was partially supported by Grant-in-Aids for Scientific Research (C) (No. 13831002) from Japan Society for the Promotion of Science, and for Scientific Research on Priority Areas (No. 14016002) from Ministry of Education, Culture, Sports, Science and Technology.

References

1. H. Kantz and T. Schreiber, *Nonlinear Time Series Analysis* (Cambridge University Press, 1997).
2. P. Grassberger and I. Procaccia, *Physica D* **9**, 189 (1983).
3. J. P. Eckmann, S. O. Kamphorst, D. Ruelle, and S. Ciliberto, *Phys. Rev. A* **34**(6), 4971 (1986).
4. F. Uesugi, Y. Tanaka, and Y. Horio, *IEICE Trans. A* **J81-A**(11), 1547 (1998), in Japanese.
5. F. Takens. *Dynamical System and Turbulence, Lecture Notes in Mathematics*, Vol. 898, eds, D. A. Rand and L. S. Young (Springer, Berlin, 1981), pp. 366–381.
6. T. Sauer, J. A. Yorke, and M. Casdagli, *J. Stat. Phys.* **65**(3/4), 579 (1991).
7. In the present paper, we describe $\log_{10}$ as common logarithm and log as natural logarithm.
8. F. Uesugi, "Influences of A–D converter on estimating Lyapunov exponents," Bachelor Thesis, Department of Electronic Engineering, Tokyo Denki University, 1996, in Japanese.

9. M. Hénon, *Commun. Math. Phys.* **50**, 69 (1976).
10. K. Judd, *Physica D* **71**, 421 (1994).
11. H. Kantz, *Phys. Rev. E* **49**(6), 5091 (1994).
12. T. Ikeguchi, *Proc. Artificial Life and Robotics*, Vol. 1 (2000), pp. 181–184.
13. The slope of this frequency distribution in log–log plots corresponds to the correlation dimension which is one of the fractal dimensions.[10]
14. K. Ikeda, *Optics Commun.* **30**(2), 257 (1979).
15. E. N. Lorenz, *J. Atm. Sci.* **20**, 130 (1963).
16. O. E. Rössler, *Phys. Lett. A* **57**(5), 397 (1976).
17. J. P. Eckmann and D. Ruelle, *Rev. Mod. Phys.* **57**(3), Part I, 617 (1985).